Quantitative Imaging of Enzymatic Vitreolysis-Induced Fiber Remodeling

Benjamen A. Filas,[1] Nihar S. Shah,[1] Qianru Zhang,[1,2] Ying-Bo Shui,[1] Spencer P. Lake,[3] and David C. Beebe[1,4]

[1]Department of Ophthalmology and Visual Sciences, Washington University School of Medicine, St. Louis, Missouri, United States
[2]Eye Center, Second Affiliated Hospital, Zhejiang University School of Medicine, Hangzhou, China
[3]Department of Mechanical Engineering and Materials Science, Washington University, St. Louis, Missouri, United States
[4]Department of Cell Biology and Physiology, Washington University School of Medicine, St. Louis, Missouri, United States

Correspondence: David C. Beebe, Department of Ophthalmology and Visual Sciences, Washington University School of Medicine, Campus Box 8096, 660 S. Euclid Avenue, St. Louis, MO 63110, USA; beebe@wustl.edu.

Submitted: July 14, 2014
Accepted: November 14, 2014

Citation: Filas BA, Shah NS, Zhang Q, Shui Y-B, Lake SP, Beebe DC. Quantitative imaging of enzymatic vitreolysis-induced fiber remodeling. *Invest Ophthalmol Vis Sci*. 2014;55:8626–8637. DOI:10.1167/iovs.14-15225

Purpose. Collagen fiber remodeling in the vitreous body has been implicated in cases of vitreomacular traction, macular hole, and retinal detachment, and also may occur during pharmacologic vitreolysis. The purpose of this study was to evaluate quantitative polarized light imaging (QPLI) as a tool for studying fiber organization in the vitreous and near the vitreoretinal interface in control and enzymatically perturbed conditions.

Methods. Fiber alignment was measured in anterior-posterior sections of bovine and porcine vitreous. Additional tests were performed on bovine lenses and nasal-temporal vitreous sections. Effects of proteoglycan degradation on collagen fiber alignment using trypsin and plasmin were assessed at the microstructural level using electron microscopy and at the global level using QPLI.

Results. Control vitreous showed fiber organization patterns consistent with the literature across multiple-length scales, including the global anterior-posterior coursing of vitreous fibers, as well as local fibers parallel to the equatorial vitreoretinal interface and transverse to the posterior interface. Proteoglycan digestion with trypsin or plasmin significantly increased fiber alignment throughout the vitreous ($P < 0.01$). The largest changes (3×) occurred in the posterior vitreous where fibers are aligned transverse to the posterior vitreoretinal interface ($P < 0.01$).

Conclusions. Proteoglycan loss due to enzymatic vitreolysis differentially increases fiber alignment at locations where tractions are most common. We hypothesize that a similar mechanism leads to retinal complications during age-related vitreous degeneration. Structural changes to the entire vitreous body (as opposed to the vitreoretinal interface alone) should be evaluated during preclinical testing of pharmacological vitreolysis candidates.

Keywords: polarized light imaging, vitreous, vitreoretinal traction, collagen, vitreous degeneration, proteoglycans, plasmin, trypsin

Comprising the bulk of the eye, the vitreous body is the colorless, acellular gel between the lens and the retina. Although 99% water, a complex network of collagen fibers, hyaluronan, and proteoglycans interact to maintain the elasticity and damping capacity of the vitreous.[1] Structural breakdown of the vitreous occurs with age, as the spaces between collagen fibers decrease and lacunae (fluid-filled pockets) form that disrupt its relatively homogeneous gel structure. Due to such age-related changes, increased stresses may develop at the vitreous periphery, leading to symptomatic vitreomacular and vitreopapillary (optic disc) traction, as well as vitreoretinal forces that may cause retinal detachment.[2] Although intimately involved in this cohort of retinal complications, the alignment of collagen fibers and how they transmit forces within the vitreous body and at the vitreoretinal interface in normal and pathophysiological circumstances is not well understood.

Much of what is known about the organization of collagen fibrils and other macromolecules in the vitreous has been derived from imaging at the microstructural level. Electron microscopy images have shown a lower density of collagen in the core of bovine vitreous relative to cortical and basal (near the ciliary body) regions,[3] corroborating earlier hydroxyproline collagen concentration assays reported by Balazs.[4] Transmission electron microscopy and high-magnification light microscopy performed on fixed human specimens have suggested that collagen fibril fragmentation may accompany age-related vitreous liquefaction.[5] High-resolution electron microscopy also has suggested important roles for chondroitin sulfate proteoglycans[6] and hyaluronan[3] in maintaining adequate spacing between the collagen fiber network, results supported by the finding that loss of type IX collagen proteoglycan side-chains occurs during age-related vitreous liquefaction.[7]

Inherent in the preceding approaches is the need for sample fixation and magnification at micrometer, or even nanometer resolution to allow for the visualization of macromolecular structure. To better understand the higher-level organization of the vitreous, alternative techniques have been used. For example, in aged human vitreous, injected colored dyes have highlighted fluid-filled lacunae,[8] and slit beam illumination has

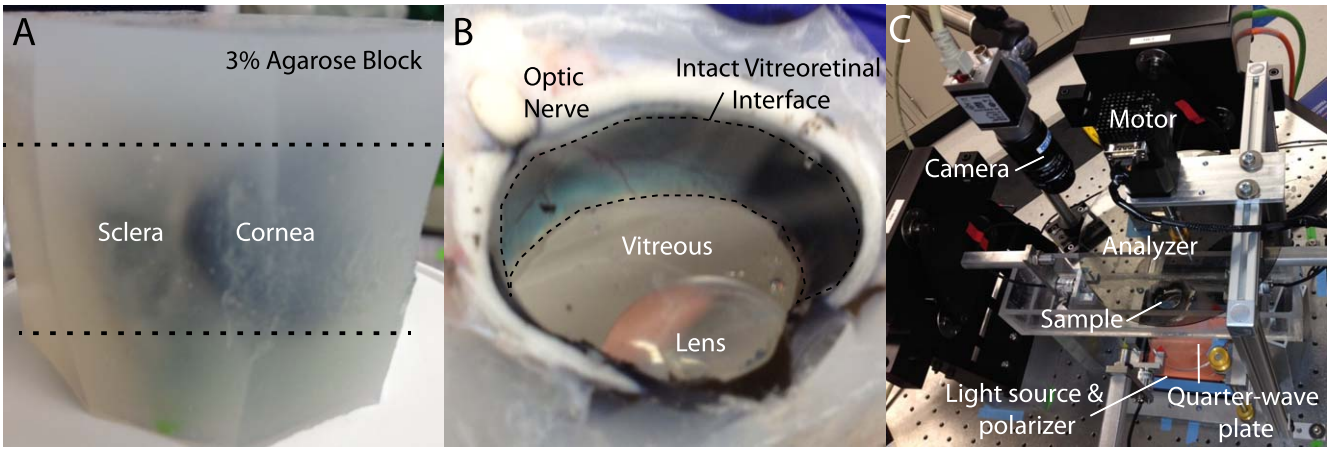

Figure 1. Experimental approach. (**A**) Eyes are cleaned of orbital tissue and embedded in agarose. (**B**) Razorblades are used to section the block at the upper and lower margins of the cornea (*dashed lines* in [**A**]) providing an optically transparent view of the vitreous and an intact vitreoretinal interface (*dashed region* in [**B**]). (**C**) The sample is placed in a tissue bath for QPLI, as previously described.[22] Further details describing this imaging technique are provided in the Methods section.

indicated collapsed and tortuous fibers.[9–11] Noninvasive ultrasound[12,13] and magnetic resonance–based[14,15] techniques also have proved useful in assessing age-related vitreous liquefaction, but are currently limited by low spatial resolution. Recent developments in swept-source optical coherence tomography have permitted noninvasive imaging of changes in vitreous organization near the retina,[16,17] but imaging elsewhere in the vitreous chamber is not currently performed with this modality.

Another technique that, to our knowledge, has not been applied to the vitreous is quantitative polarized light imaging (QPLI).[18,19] Because collagen fibrils selectively retard light perpendicular to their long axis, a net directional anisotropy in refractive index (birefringence) is present in samples with larger-scale structural order.[20] Plane polarized light undergoes changes in phase when passing through birefringent medium, allowing the calculation of retardation (proportional to net fiber alignment) and the principal direction of the alignment.[20] This approach provides a noninvasive, submicroscopic assessment of fiber organization that is well-suited for the characterization of thick, weakly aligned, optically transparent tissues.[18] Practical examples of this approach applied to semitransparent samples include dynamic imaging during the mechanical testing of biomimetic tissue equivalents,[21,22] tendons,[23] and ligaments.[24]

The objective of this study was to evaluate the suitability of the QPLI technique in characterizing intact vitreous and use it to provide insight into the effects of enzymatic vitreolysis on gross vitreous structure. Although we found relatively low optical retardation values (fiber alignment) in control bovine and porcine vitreous, we identified repeatable and consistent patterns of fiber alignment and orientation between species, consistent with previous microstructural studies. To support our results, we show that the technique reliably characterizes the highly ordered structure of the bovine lens, including the presence of Y-shaped sutures and radially aligned fiber cells.[25,26] Next, we use the approach to characterize vitreous treated with trypsin or plasmin. Despite approval by the Food and Drug Administration in 2012,[27] the effects of ocriplasmin (a smaller, recombinant version of plasmin but with the same active domain) on gross vitreous fiber organization remain unknown, as the effects of this enzyme are generally only screened at the microstructural level in animal studies[28–30] or imaged intermittently with optical coherence tomography near the vitreomacular interface in human patients.[27] Because of this, the mechanism of enzymatic-vitreolysis–induced resolution of vitreoretinal tractions is not well understood.[31] Results from this study indicate that trypsin or plasmin treatment increases collagen fiber alignment throughout the vitreous, and most significantly in the posterior vitreous, near sites such as the optic disc (bovine and porcine eyes do not have a macula). These results show that the reorganization of vitreous fibrils via the digestion of proteoglycans may play a larger role in plasmin-induced enzymatic vitreolysis than previously appreciated. Implications for these results in the resolution of vitreomacular tractions, as well as the off-label use of ocriplasmin to treat diabetic macular edema and age-related macular degeneration are discussed.

Methods

Sample Preparation

Fresh bovine and porcine eyes were obtained immediately after animals were killed (Trenton Processing, Trenton, IL, USA) and transported to Washington University on ice (<1 hour). Because samples needed to be mechanically sectioned to provide optically transparent samples for QPLI, eyes were first cleaned of excess orbital tissue and embedded in 3% agarose to provide stability (Fig. 1A). Samples were added to the cooling agarose once body temperature was reached. After the agarose solidified, a large razor blade (Edge-Rite high-profile microtome blade; Thermo Scientific, Waltham, MA, USA) glued to a plastic coverslip (5 × 5 cm) was used to cut the eye beginning at the margin of the cornea in the anterior-posterior direction (dashed lines in Fig. 1A). The sample was then inverted (the vitreous would not fall out due to the presence of the coverslip) and the procedure was repeated, providing a thick, optically transparent sample with an intact vitreoretinal interface (Fig. 1B). In other experiments, to probe fiber alignment perpendicular to the anterior-posterior axis, the direction of the cuts was changed from the anterior-posterior to the nasal-temporal direction. In both orientations, the intact lens could be removed and imaged in isolation.

Enzyme Treatments

Trypsin was used to digest proteoglycans, and to a lesser degree, some collagens (e.g., chondroitin-associated regions of

Investigative Ophthalmology & Visual Science

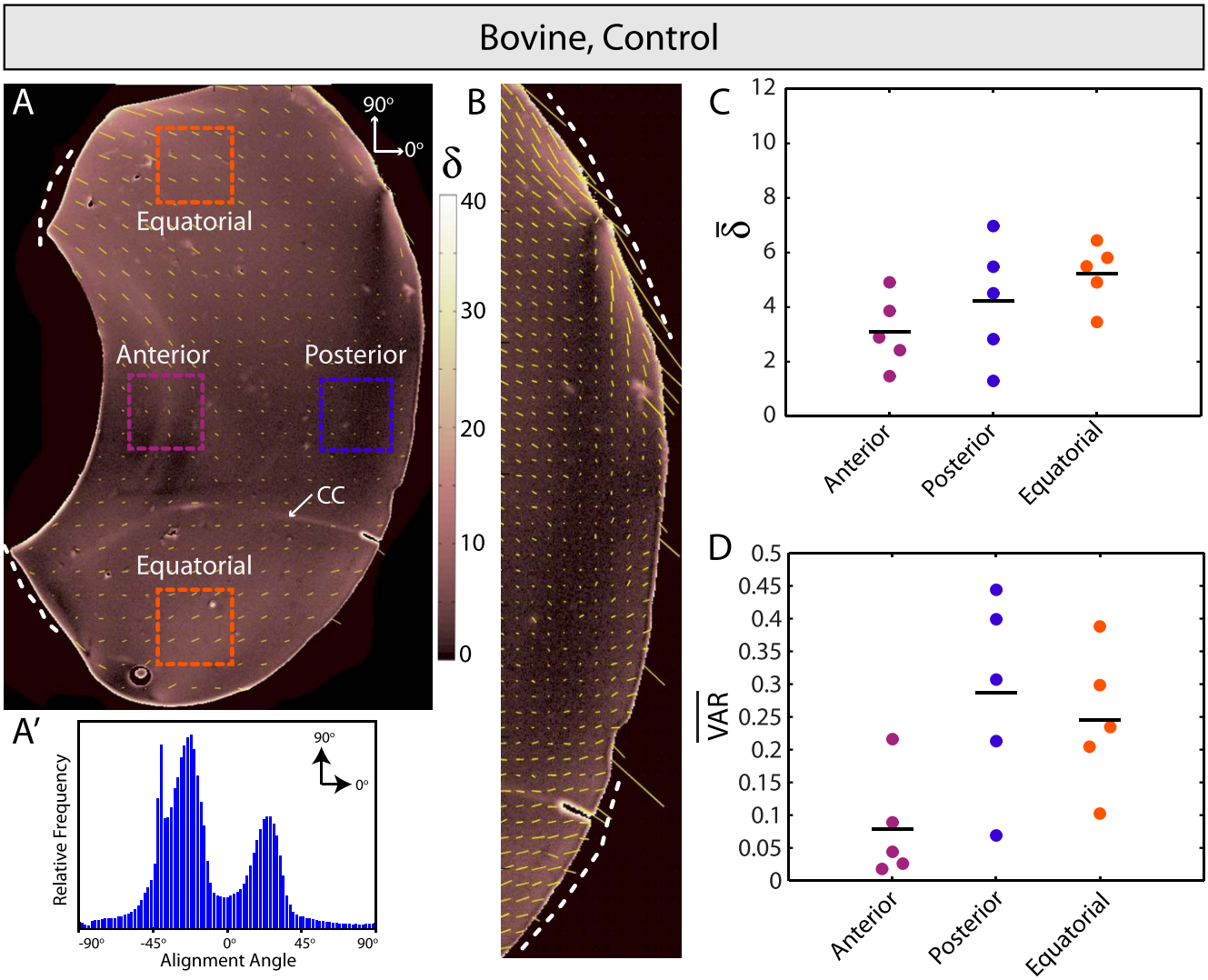

Figure 2. Control bovine vitreous. (**A**) Spatial map of fiber alignment strength (retardation, δ) and scaled orientation (*yellow vectors*). *Dashed lines* indicate the vitreous base and the *arrow* shows the location of Cloquet's canal (CC). (**A′**) Relative frequency histogram for alignment angles in (**A**). Bimodal peaks in alignment angle reflect bilateral sample symmetry. (**B**) High-resolution image of posterior vitreous. Fibers are oriented parallel to the retina in equatorial locations (*dashed lines*) and transverse further posterior. (**C**, **D**) Average retardation ($\bar{\delta}$) is highest and lowest in equatorial and anterior vitreous, respectively, but differences were not statistically significant. Similarly, no significant differences in average circular variance ($\overline{VAR}$) were observed between regions.

collagen IX and non–triple helical regions of collagen II).[1,7,32] Although often referenced as specific for fibrin and laminin, plasmin is a member of the trypsin protease family (provided in the public domain by http://www.brenda-enzymes.org/php/result_flat.php4?ecno=3.4.21.7), and cuts at the same basic amino acids (Arg, Lys) as trypsin, albeit with higher substrate specificity. Proteomics-grade purified trypsin (1 μg/mL, T6567, 109K6120; Sigma-Aldrich Corp., St. Louis, MO, USA) or plasmin (0.2 U/mL, #527624, D00139129; EMD Millipore, Billerica, MA, USA) diluted in PBS containing calcium and magnesium chloride (final injection volume: 300 μL) was injected into the vitreous with a 30-gauge needle, and samples were incubated overnight at 37°C before QPLI. Noticeably different results were not observed when enzymes were twice as concentrated and the same injection and incubation protocol was followed. Moreover, PBS sham injections showed negligible difference relative to uninjected eyes. In a separate set of experiments, trypsin was injected, but samples were imaged after only 10 minutes or 1 hour of incubation.

Quantitative Polarized Light Imaging

A custom QPLI system (Fig. 1C) was used to acquire high-resolution maps of collagen alignment (retardation, δ) and orientation in the vitreous, as previously described.[22] Briefly, a fiber light source and a linear polarizer sheet (Edmund Optics, Barrington, NJ, USA) provided wide-field sample illumination through a quarter-wave plate (Bolder Vision Optik, Inc., Boulder, CO, USA) while images were acquired with a charge-coupled device camera (Basler, Exton, PA, USA) and a circular analyzer controlled by a step motor (total image acquisition time was approximately 2 seconds per alignment map; Fig. 1C). Light intensity was kept constant within each species to ensure appropriate comparison of retardation values between samples. Sample thickness varied slightly (bovine:

Investigative Ophthalmology & Visual Science

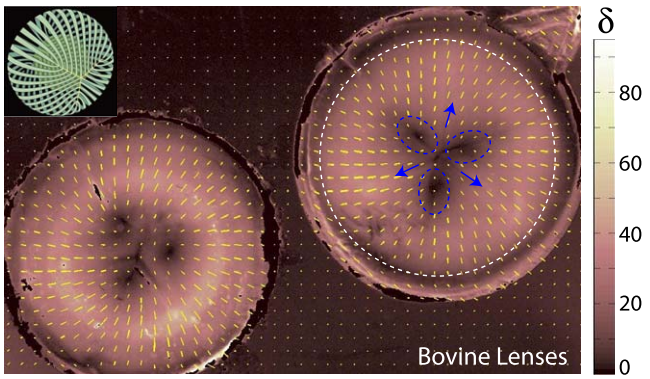

FIGURE 3. Bovine lenses. *Inset*: Reference schematic for lens suture (*yellow* "*Y*") and fiber cell organization (*green*) in the bovine lens (adapted from Kuszak JR, Zoltoski RK, Sivertson C. Fibre cell organization in crystalline lenses. *Exp Eye Res*. 2004;78(3):673–687. Copyright © 2003 Elsevier Science Ltd.). (*Left*, *right*) Two bovine lenses. The lens on the *right* is annotated. Fiber cells are oriented radially in all locations and retardation (δ) is substantially higher than vitreous samples. Y-shaped sutures are present (*blue arrows*) and regions of reduced retardation (*dashed blue circles*) are found between suture lines. Another zone of reduced retardation is located near the lens periphery (*dashed white line*). Both regions correspond to locations where fiber cells presumably curve out of the imaging plane.

15–20 mm; porcine: 9–12 mm), but no intrasample variation in retardation was seen within these ranges of thickness.

Deep-Etch Electron Microscopy (DEEM)

To characterize vitreous microstructure absent of fixation artifacts, DEEM was performed as previously described,[33] with minor modifications. Briefly, a small drop of central core vitreous was placed onto a coverglass and sandwiched with a 0.5-mm thick, 3-mm diameter sapphire glass. The sample was then frozen by forceful impact against a pure copper block, and cooled to 4°K with liquid helium. Frozen samples were transferred to an evaporator and freeze fracture occurred by removing the sapphire cover slip at −104°C under vacuum. Samples were etched for 2 minutes and rotary replicated with approximately 3 nm platinum. Resulting replicas were photographed on a JEOL 1400 transmission electron microscope (JEOL USA, Inc., Peabody, MA, USA) with an AMT XR111 digital camera (AMT Corp., Woburn, MA, USA).

Data Analysis and Statistics

A custom Matlab (v2014a; Mathworks, Natick, MA, USA) graphical user interface was written for quantitative analysis of retardation and fiber alignment in the vitreous. First, birefringent tissue outside of the vitreous was manually removed from the images (such as the lens) and high-intensity reflection artifacts above a specified threshold were excluded. The average retardation and circular variance (calculated using the circular statistics toolbox)[34] was determined for the entire vitreous, and resulting angle alignment histograms were binned into 2° increments. Note that, although the average retardation is proportional to the microscopic fiber alignment at a particular pixel, the circular variance refers to a more global measure of fiber direction averaged across thousands of pixels. Similarly, local measures (approximately 5 × 5-mm regions) of retardation and circular variance were made in three vitreous locations: anterior (behind the lens), posterior (in front of the retina), and equatorial (at the sides of the vitreous) (e.g., see Fig. 2A). Due to symmetry, equatorial values were computed for two locations and averaged for subsequent statistical testing. In samples cut perpendicular to the anterior-posterior axis, local quantification regions included the vitreous core and four locations at the periphery. Again, owing to symmetry, data from the four periphery locations were averaged before further analysis.

One-way ANOVA, with post hoc pairwise comparison made with the Bonferroni-Dunn test, was used to compare anterior, posterior, and equatorial locations within each sample, as well as across perturbation groups (control, trypsin, and plasmin) in each region. A two-tailed Student's *t*-test was used to compare differences between core and periphery locations in the equatorial bovine sections. Results are plotted as raw data, with the mean indicated by a black bar and $P < 0.05$ denoting statistical significance. All experiments were performed, at a minimum, in triplicate, with specific numbers for each set provided in the Results section.

RESULTS

Quantitative Polarized Light Imaging Shows Global Patterns of Fiber Alignment in Bovine and Porcine Vitreous

First, we used QPLI to assess fiber alignment in control bovine and porcine vitreous (Fig. 2, Supplementary Fig. S1; $n = 5$ and 4, respectively). Consistent with earlier slit illumination studies in younger human eyes,[11] we found relatively uniform patterns of fibers coursing in the anterior-posterior direction (dashed lines, Fig. 2A, Supplementary Fig. S1A) from the vitreous base toward the posterior side. Average vitreous retardation was low ($\bar{\delta} < 10$; for comparison, acellular 1 mg/mL collagen-agarose co-gels averaged values between 15 and 30),[21] and global fiber orientation patterns were bimodal (Fig. 2A′, Supplementary Fig. S1A′), reflecting the bilateral symmetry present in the samples. Due to size, shape, and other possible species-related differences, the peaks of the bimodal angle distributions differed by approximately 30° between the two groups.

Fiber orientation was mostly transverse to the wall at the vitreous base, supporting earlier histology studies showing fiber insertion through the internal limiting membrane in this region.[35,36] Fibers were similarly directed transverse to the wall in the posterior vitreous, but were parallel in orientation in more equatorial regions (Fig. 2B, Supplementary Fig. S1B), again consistent with past slit lamp[11] and histological findings.[35–37] Average alignment angle for all samples (measured between −90° and +90° with 0° corresponding to an anterior-posterior orientation, see Fig. 2A) for the anterior, posterior, upper equatorial, and lower equatorial regions were 3.8 ± 10.8°, −1.0 ± 10.5°, −33.4 ± 9.3°, and 35.6 ± 13.6°, respectively. The average difference in orientation between equatorial regions was 69.0 ± 16.4°. Although at times difficult to distinguish from the sample wall, a thin layer of increased retardation near the vitreous border was suggestive of a cortical layer (Figs. 2A, 2B; Supplementary Figs. S1A, S1B).[38] No significant differences in average retardation or circular variance were found in anterior, posterior, and equatorial vitreous regions (Figs. 2C, 2D; Supplementary Figs. S1C, S1D), but general trends were similar between species, with the highest average retardation, or microscopic fiber alignment, observed equatorially and the lowest behind the lens. Last, we note that, although we have used dye injections to confirm the presence of (a very small) Cloquet's Canal in bovine vitreous (Zhang Q, unpublished observation, 2012), this structure was only sometimes visible in the polarized light images (arrow in Fig. 2A), potentially due to sectioning location.

Investigative Ophthalmology & Visual Science

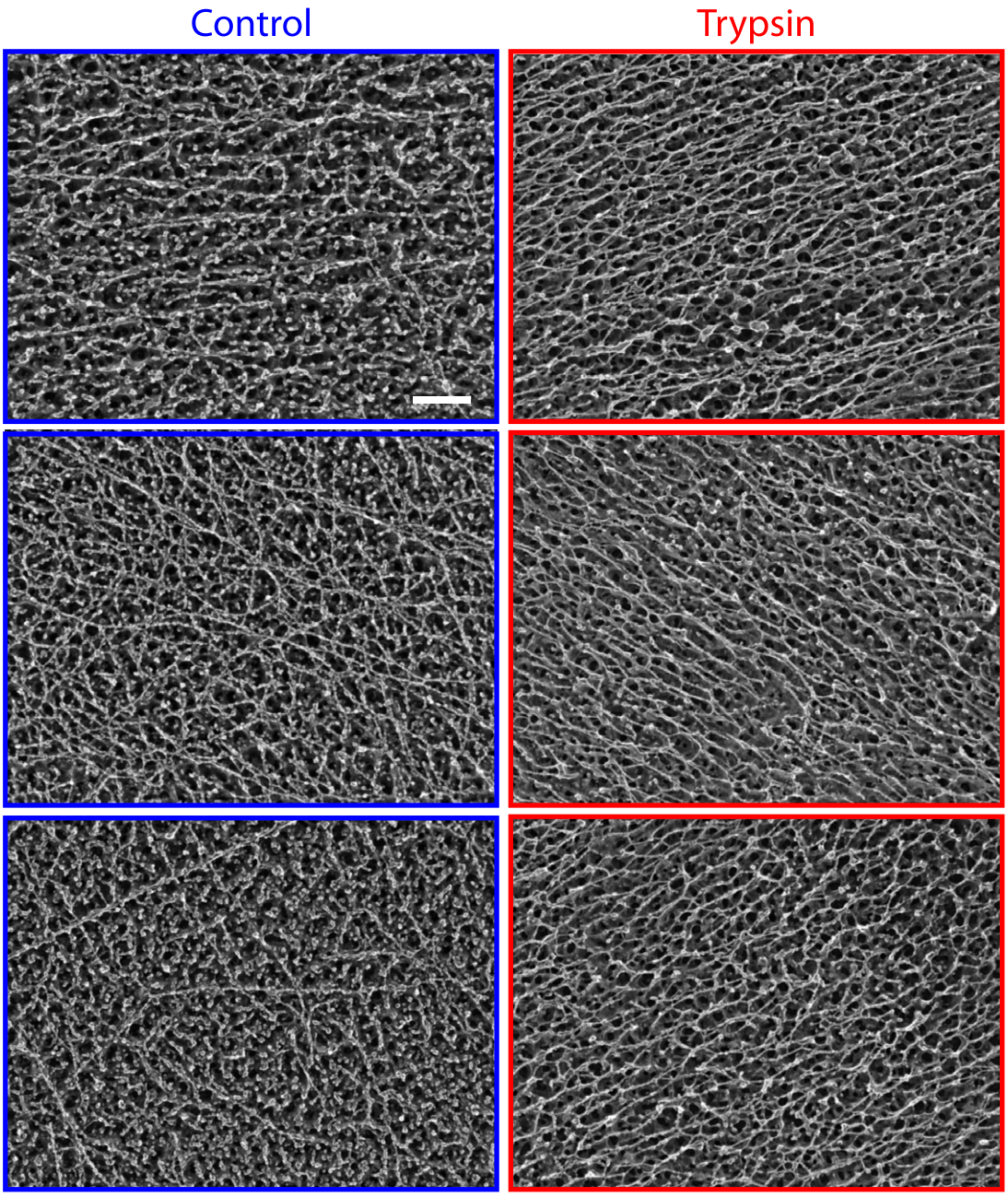

FIGURE 4. Deep-etch electron microscopy. *Left*: Representative images of control bovine vitreous from three different eyes. A complex network of fibers and globules comprise vitreous microstructure. *Right*: Representative images of trypsin-treated bovine vitreous from three eyes. Globule concentration (presumed soluble proteins and proteoglycans) is substantially reduced. Remaining fibers are more uniformly aligned. *Scale bar*: 100 nm.

Additional QPLI Tests

Reproducible patterns in fiber alignment and orientation between bovine and porcine vitreous consistent with the literature indicated QPLI to be a reasonable approach for imaging collagen fibers in the vitreous and near the vitreoretinal interface. To test the method further, we first imaged bovine lenses in isolation ($n = 6$). Due to the high reflectivity of these samples, lenses were submerged in PBS before imaging. Although no extracellular matrix is present between them, the specialized fiber cells of the lens are some of the most elongated, organized, optically transparent, and tightly packed in the body, making them well-suited for polarized light imaging.[39] Quantitative polarized light imaging clearly showed the presence of the Y-shaped sutures (blue arrows, Fig. 3) in bovine lenses that act as junctions between the apical and basal ends of the fiber cells. Lens fiber cell retardation was substantially higher than the vitreous ($\delta \approx 40$–80), and orientation was radial throughout, consistent with well-described lens fiber cell geometries (Fig. 3, inset).[26,39] Regions of reduced retardation between suture lines (Fig. 3, dashed blue ovals) were observed, as was lower retardation near the edge of the lens (Fig. 3, dashed white line), likely indicative of cells curving out of the imaging plane. These results were consistent independent of whether or not the cortical cell layer was removed (not shown).

Investigative Ophthalmology & Visual Science

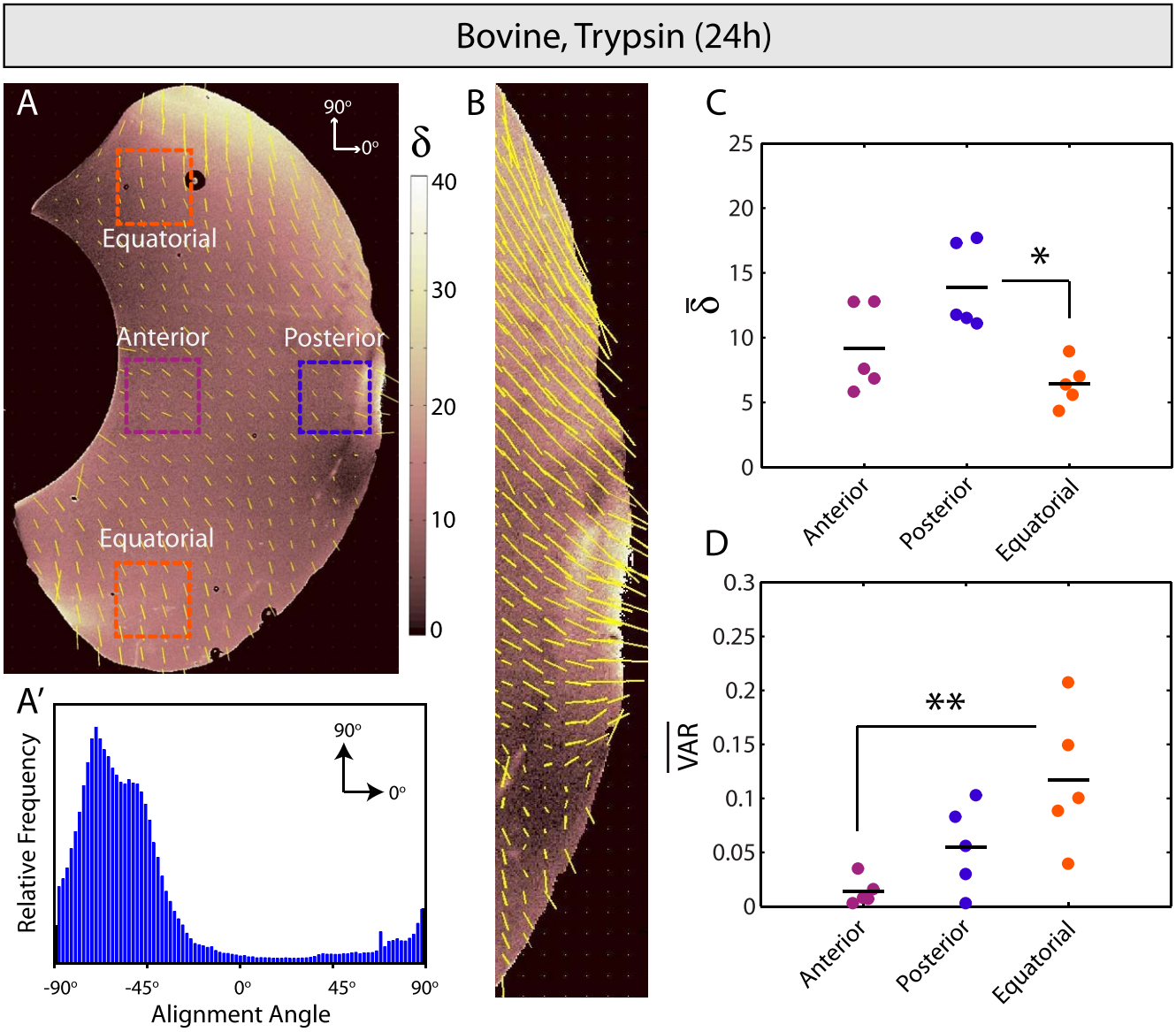

Figure 5. Enzymatic vitreolysis with trypsin. (**A**, **A′**) Optical retardation (δ, indicating microscopic fiber alignment) is higher and the global orientation of remaining fibers is more homogeneous than bovine controls. (**B**) Fibers are aligned most strongly and in a transverse orientation to the vitreoretinal interface in the posterior vitreous. (**C**) Fibers are significantly more aligned in the posterior as compared to equatorial vitreous ($P < 0.05$). (**D**) Circular variance indicates significantly less anisotropy in the equatorial versus anterior vitreous ($P < 0.01$).

In a separate test, we cut and imaged bovine vitreous samples in a nasal-temporal (as opposed to anterior-posterior) orientation ($n = 5$). Microscopic fiber alignment (retardation) was slightly higher than in the anterior-posterior cuts, and fibers were homogeneously oriented in a largely vertical orientation throughout the sample (Supplementary Fig. S2). Hence, global alignment histograms displayed a single peak (Supplementary Fig. S2A′), and low circular variance values ($VAR < 0.05$, Supplementary Fig. S2C) were found in both the vitreous core and periphery. Extrapolating to three dimensions, these findings were consistent with our earlier results in that both the nasal-temporal (Supplementary Fig. S2) and anterior-posterior imaging data (Fig. 2) suggest that vitreous fibers course in the anterior-posterior direction at an inclined angle from the vitreous base toward the middle of the posterior vitreous.

Together, results from control bovine and porcine vitreous, bovine lenses, and nasal-temporal sections of bovine vitreous suggested QPLI to be a reliable technique for imaging fiber alignment in optically transparent ocular samples. Because we found good agreement between QPLI results and other imaging modalities used in past studies, we next used QPLI to quantitatively characterize the unknown effects of enzymatic vitreolysis on gross vitreous structure.

Vitreous Fibers Are Most Strongly Aligned Near the Posterior Vitreoretinal Interface After Proteoglycan Degradation

Previously, we showed that digesting proteoglycans with trypsin decreases the elastic storage modulus (or stiffness) of the vitreous.[1] Further investigation at the microstructural level using DEEM revealed that trypsin treatment results in the

Investigative Ophthalmology & Visual Science

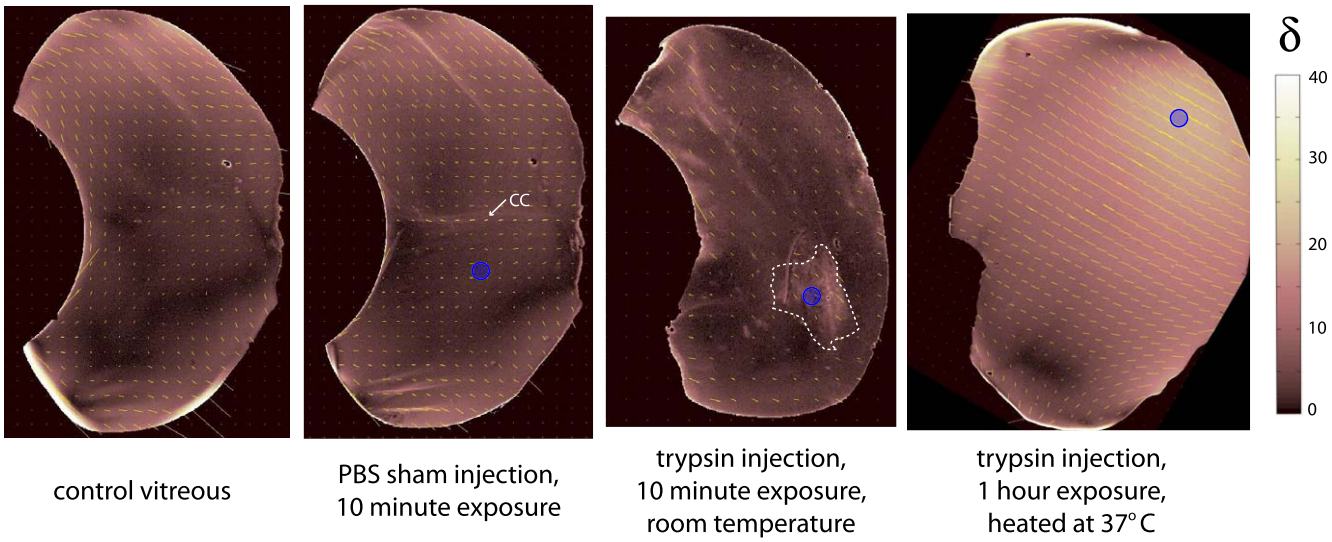

Figure 6. Vitreous injected with PBS and trypsin. Cutting plane was anterior to posterior. *Blue circles* indicate approximate injection location. (*Left* and *Middle-Left*) Control vitreous before and after 300-μL PBS injection. Fiber alignment does not change, but Cloquet's canal (CC) is more visible. (*Middle-Right*) Trypsin injection increases fiber alignment locally (*dashed white line*) after 10-minute exposure at room temperature. (*Right*) A region of increased optical retardation (δ) is still visible near the trypsin injection site after 1 hour of heated incubation. Global fiber alignment and orientation patterns are different from overnight incubations (see Fig. 5), suggesting incomplete structural remodeling.

increased alignment of remaining vitreous fibers and the concomitant loss of circular globules (presumed soluble proteins and proteoglycans) attached to the fibers (Fig. 4, $n = 6$). However, it remained unclear how these microstructural changes in alignment affected gross patterns of fiber organization throughout the vitreous, and importantly, near the vitreoretinal interface.

After trypsin injection and overnight incubation, QPLI revealed significantly different patterns in fiber alignment and orientation relative to controls (Figs. 2, 5; $n = 5$). Fiber alignment increased throughout, most significantly in the posterior vitreous near the vitreoretinal interface (Figs. 5A, 5C). Clear bimodality was no longer present in the global fiber alignment distribution (Fig. 5A′), but orientation patterns were similar to controls near the retina (parallel orientation equatorially, transverse orientation further posterior; Fig. 5B). Average fiber orientation was $-4.2 \pm 19.3°$ and $-7.9 \pm 15.8°$ in the anterior and posterior vitreous, respectively. Although the average angles in the upper and lower equatorial regions were highly variable in the trypsin-treated samples, a consistent trend was low differences in average angle between these two sampling locations. The average difference in dominant orientation angle between equatorial regions was $13.9 \pm 10.7°$ (as compared to $\sim 70°$ in controls), a result reflected in the loss of bimodality that was found in the global fiber alignment distributions for these samples. Notably, fiber orientation was most variable in the equatorial vitreous and least variable in the anterior vitreous behind the lens (Fig. 5D). To help confirm that trypsin treatment remodels and aligns vitreous fibers, we repeated the experiment but incubated eyes for reduced times. An apparent locus of increased fiber alignment was present near the injection site (blue circle, Fig. 6, $n = 3$), a result that was not observed in PBS sham controls. Together, these results, in combination with the DEEM images, suggested that proteoglycan digestion via trypsin treatment aligns vitreous fibers throughout the vitreous, with the most significant changes occurring near the vitreoretinal interface.

The overnight enzymatic vitreolysis protocol was then repeated using plasmin ($n = 8$). Results were similar to trypsin-treated vitreous, including increased fiber alignment and less bimodality in the fiber orientation histograms relative to controls (Figs. 7A, A′). Again, maximal fiber alignment was transverse to the vitreoretinal interface in the posterior vitreous (Figs. 7B, 7C), whereas the greatest angular variation was in the equatorial vitreous (Fig. 7D). Similar to the trypsin results, average anterior and posterior angles were $-15.3 \pm 14.8°$ and $-4.9 \pm 18.0°$ with only small differences in average orientation ($17.6 \pm 13.9°$) present between the more variable equatorial regions.

Quantitative comparison of anterior-posterior bovine sections indicated significant differences between groups (control, trypsin, plasmin; Fig. 8). Fibers were significantly more aligned with tighter angle distributions in trypsin- and plasmin-treated samples relative to controls (Fig. 8, top row). Interestingly, this trend was consistent in the anterior and posterior vitreous, but no significant differences in retardation were observed across groups in the equatorial vitreous (Fig. 8, rows 2–4). Similarly, angular variation was significantly lower in anterior and posterior vitreous in the enzyme-treated samples but not in equatorial vitreous (Fig. 8, rows 2–4). Although no significant differences were found either globally or locally between the trypsin and plasmin-treated samples, we note that, in general, plasmin-induced remodeling was not as pronounced as trypsin (δ lower in all regions analyzed, Fig. 8).

Discussion

In this study, we demonstrated the utility of QPLI in analyzing fiber distributions in the vitreous body and near the vitreoretinal interface. Results suggest that enzymatic digestion of proteoglycans differentially aligns fibers throughout the vitreous body. In particular, alignment is strongest in the posterior vitreous, where fibers are oriented transverse to the vitreoretinal interface. These findings suggest that proteoglycan loss due to enzymatic vitreolysis causes structural remodeling in the vitreous marked by increased collagen fibril alignment. Implications for these findings in the etiology and treatment of vitreoretinal tractions are discussed.

Investigative Ophthalmology & Visual Science

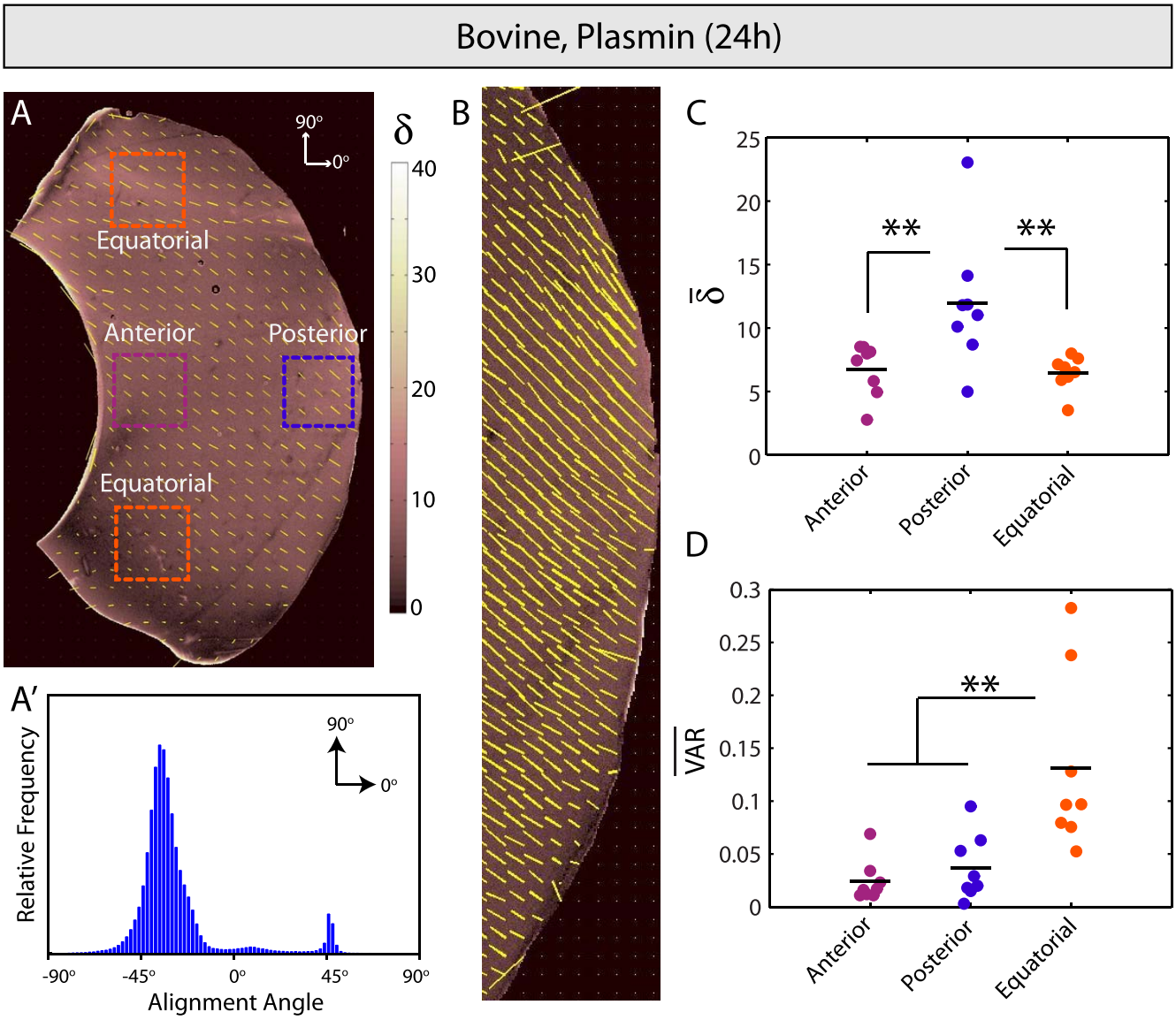

Figure 7. Enzymatic vitreolysis with plasmin. (**A**, **A′**) Microscopic fiber alignment (optical retardation, δ) is elevated throughout and fiber orientation is relatively homogeneous. (**B**, **C**) Fibers are significantly more aligned transverse to the vitreoretinal interface in the posterior vitreous compared with other regions ($P < 0.01$). (**D**) There is significantly less angular variation in the anterior and posterior vitreous relative to the equatorial vitreous ($P < 0.01$).

Quantitative Polarized Light Imaging Captures Global Patterns of Vitreous Microstructure

In a previous study, we used extensional rheometry to study the effects of enzymes on the adhesivity of the vitreous body,[1] but the effects of collagen fiber organization and remodeling could not be assessed using this approach. Quantitative polarized light imaging provides an imaging tool in which fiber organization can be measured throughout the vitreous body, including near the vitreoretinal interface, in normal and enzymatically perturbed conditions. Using this technique, we were able to capture morphological details of the vitreous at both global (anterior-posterior coursing of organized collagen fibers), and local levels (transverse fiber orientation at the vitreous base and posterior vitreous and parallel orientation in the equatorial vitreous) (Fig. 2, Supplementary Fig. S1). Quantitative polarized light imaging tests on the highly ordered bovine lens confirmed the presence of radially aligned fiber cells and three suture planes (Fig. 3), whereas tests on nasal-temporal vitreous sections indicated a relatively homogeneous fiber alignment pattern (Supplementary Fig. S2). Subsequent tests provided additional evidence that enzyme-induced proteoglycan digestion aligns the remaining vitreous fibers (Figs. 5–7), a result that was initially suggested by DEEM studies (Fig. 4).

These data suggest that the comparatively lower fiber alignment values observed in control vitreous are due to proteoglycans and other macromolecules providing spacing between the fibers. This interpretation is supported by the DEEM images showing circular globules (presumed proteoglycans) present between well-spaced and more randomly oriented fibers in control vitreous and aligned fibers lacking globules in trypsin-treated samples (Fig. 4). In control vitreous we found that the lowest anterior-posterior fiber alignment was present in the vitreous core behind the lens (Fig. 2A, Supplementary Fig. S1A), a region where the first signs of age-

Investigative Ophthalmology & Visual Science

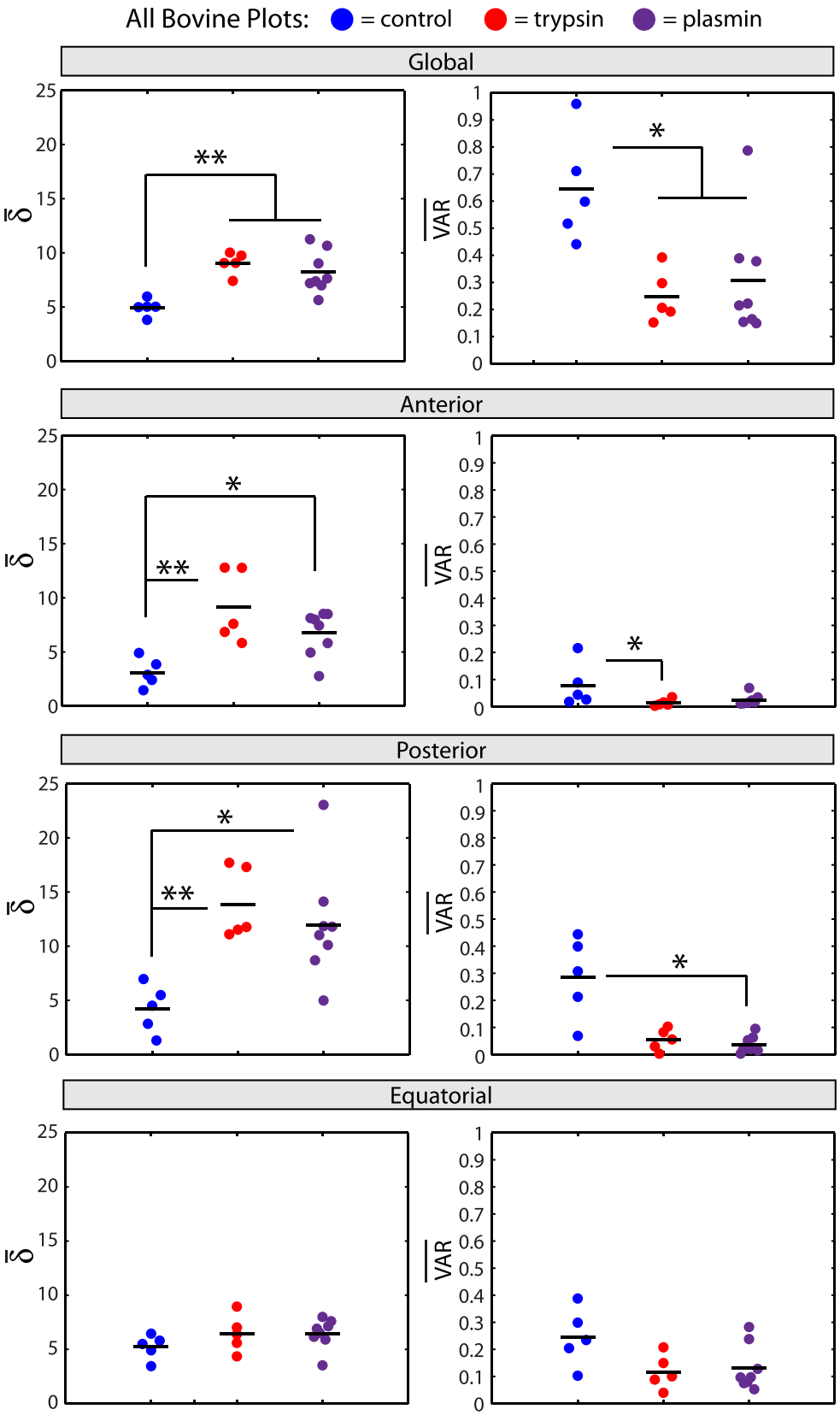

Figure 8. Quantitative bovine vitreous comparison. Average retardation ($\bar{\delta}$) and circular variance ($\overline{VAR}$) from all anterior-posterior bovine sections in the three treatment groups (control, *blue*; trypsin, *red*; plasmin, *purple*) and four sampling locations (global, *top row*; anterior, *second row*; posterior, *third row*; equatorial, *bottom row*) are shown. Fibers are significantly more aligned ($P < 0.01$) and homogeneously oriented ($P < 0.05$) in control relative to enzyme-treated vitreous (*top row*). This trend is the same in anterior and posterior vitreous (second and third rows, $^{**}P < 0.01$, $^{*}P < 0.05$), but no significant differences between groups are present in equatorial vitreous (*bottom row*).

Investigative Ophthalmology & Visual Science

related liquefaction are detected in humans.[40] Higher fiber alignment was found in the equatorial vitreous near the ciliary body where vitreoretinal adhesion is strongest.[35,36] Similar levels of alignment were detected in nasal-temporal sections where fibers appear to enter and exit the imaging plane at a consistent but slightly inclined angle due to overall eye geometry (Supplementary Fig. S2). Average retardation was not lower in the core relative to the periphery of the nasal-temporal sections as was found in the anterior-posterior sections. This indicates possible anisotropic differences in microstructural fiber alignment in this region. An alternative explanation is that cutting the major anterior-posterior fibers caused fibers to align (e.g., via collapse) in the nasal-temporal orientation. Future studies characterizing how vitreous structure dynamically changes in response to mechanical perturbations could be useful in gauging this potential effect.

Differential fiber alignment in the anterior-posterior direction of control vitreous indicated that the response to proteoglycan degradation in this tissue may not end up being uniform. Images of trypsin-injected samples at shorter incubation times showed a locus of increased fiber alignment (Fig. 6) near the injection site, a result that differed considerably from the fiber alignment patterns observed after 24 hours of incubation (Fig. 5). These data suggest that local collagen remodeling precedes the global fiber reorganization that occurs once the enzyme is more fully diffused. After 24 hours, fiber alignment increased throughout the vitreous and similar regional trends were observed between plasmin- and trypsin-treated samples (Fig. 8). These data support QPLI as a useful tool to study the time-varying effects of enzyme-induced vitreous remodeling.

Although the focus of the current study was to establish the QPLI technique in the vitreous and use it to characterize the effects of enzymatic-induced proteoglycan degradation, a potential future application of this method is to dynamically image global and local collagen alignment patterns. For example, studies combining QPLI and mechanical testing (e.g., uniaxial and biaxial stretching) would be useful in deciphering the role of collagen fiber orientation and alignment in transmitting forces across the vitreous to the vitreoretinal interface. Such information could be helpful in optimizing surgical procedures to minimize vitreoretinal traction,[41] designing pharmacological vitreolysis agents,[31,42] and improving biomechanical impact models. For example, in the latter case, finite-element models have been developed in an attempt to explain pathogenic mechanisms of blast or shaken baby–induced retinal trauma, while modeling the vitreous as a homogeneous viscoelastic material.[43–45] Because the structural organization of the vitreous and the vitreoretinal interface also can affect the retina,[2] incorporating anisotropic collagen alignment and orientation data in the vitreous could aid in improving the biological accuracy and predictive ability of such simulations.

Characterizing the vitreous with QPLI is not without limitations. The technique requires an optically transparent sample that, at present, necessitates ex vivo analysis and cutting of the sclera. Consistent alignment patterns in the anterior-posterior sections (Fig. 2), however, suggested that the physical act of cutting does not substantially affect results. On the other hand, we found it difficult with the current method to perform accurate cuts (even after embedding) using smaller eyes with a less fibrous sclera, such as the rabbit. Another limitation is that QPLI does not explicitly differentiate between multiple fiber populations.[22] Due to the highly birefringent properties of collagen and the similarity of our results with past studies of collagen organization,[35,40,46] however, we assume that collagen remodeling is the primary factor affecting the QPLI data reported here.

Insight Into Causes of Age-Related Vitreous Degeneration and Vitreoretinal Tractions

Increased collagen disorganization and a transition from a gel-like to a liquid vitreous are common outcomes due to age-related vitreous degeneration. As the vitreous liquefies and collapses, the risk for symptomatic tractions in well-adhered regions between the vitreous and the retina increases. Mechanistically, little is known about the causes of age-related vitreous degeneration in humans. The only age-related change in vitreous protein structure that has been reported is the loss of type IX collagen proteoglycan, which also results in the increased exposure of type II collagen fibrils (to which the type IX collagen was originally bound).[7] Because type II collagens have a tendency to aggregate, it was hypothesized that this process could be involved in the formation of the larger collagen fibers observed in aged human vitreous.

Similarly, enzymatic digestion of proteoglycans using trypsin or plasmin increased fiber alignment throughout the vitreous body (Figs. 5, 6). At the microstructural level, high-resolution electron microscopy imaging showed increased alignment of linear fibers due to the loss of the circular globules that were originally attached to these fibers (Fig. 4). These results suggest that proteoglycan loss results in increased structural anisotropy and exposure of vitreous fibers, which could predispose them to later agglomeration. Importantly, however, our QPLI data show that increases in fiber alignment are not homogeneous throughout the vitreous. For example, in the equatorial vitreous, where fiber alignment is strongest in controls (Fig. 2A), fiber alignment slightly increases in plasmin and trypsin-treated vitreous relative to controls, but this change is small and not statistically significant (Fig. 8, bottom row). On the other hand, in the two regions with lower initial retardation, fiber alignment increased approximately 2-fold in the anterior and 3-fold in the posterior vitreous (Fig. 8, second and third rows). The disproportionate increase in fiber alignment in this experiment, especially transverse to the posterior vitreoretinal interface, provides potential insight into the mechanism of vitreoretinal traction in humans. First, age-related loss of collagen-II spacing molecules, such as proteoglycans, reduces the elasticity of the vitreous.[1] As the vitreous is degraded, the vitreous remains attached to the posterior retina at sites where adhesion is stronger (e.g., at the macula or the optic disc). This increases collagen fiber alignment in these regions as fibers are pulled together at an orientation transverse to the adhesive site. We speculate that the net result of these structural changes would be an increase in vitreoretinal traction in the affected region.

Clinical Implications

Plasmin is a nonspecific serine protease in the same class of enzymes as trypsin, which cleaves peptide bonds after the basic residues arginine and lysine. Because of this ubiquity, plasmin degradation plays a role in many physiological processes, including angiogenesis, embryogenesis, wound healing, tumor cell invasion, and extracellular matrix remodeling.[47] Hence, it is reasonable that plasmin caused significant fiber remodeling throughout the vitreous (Fig. 7) and that these changes were similar to those induced by trypsin (Figs. 5, 8). Global effects of plasmin on the vitreous body outside the vitreoretinal interface have been reported elsewhere. Sebag et al.[48] showed enhanced nanosphere diffusion in the vitreous after treatment with microplasmin (a shorter version of plasmin with the same proteolytic domain; now called ocriplasmin). Moreover, increased oxygen content in the vitreous body and in the lens after plasmin or microplasmin treatment has been reported by a number of investigators,[49–51]

Investigative Ophthalmology & Visual Science

results indicative of increased vitreous liquefaction and enhanced intravitreal transport between the retina and the lens.[39,52]

Often, ocriplasmin substrates are cited as "fibronectin and laminin, components of the vitreoretinal interface,"[27] but as noted by Bishop,[31] it is unclear whether laminin and fibronectin are directly involved in vitreoretinal adhesion. Our results support a nonspecific mechanism of plasmin vitreolysis where proteoglycan digestion reduces the elasticity of the vitreous[1] and aligns remaining vitreous fibers. Due to local differences in vitreoretinal adhesion strength[53] and sample geometry, proteoglycan degradation causes spatially varying changes in fiber organization (Figs. 5, 7), with alignment increased most significantly in the posterior vitreous at an orientation transverse to the vitreoretinal interface (Fig. 8). From these data, we speculate that, in cases of persistent vitreoretinal adhesion, vitreous shrinkage and increased fiber alignment at the vitreoretinal interface could lead to increased mechanical traction. Such a result may be beneficial in the management of small tractions, where the combined effects of the enzyme liquefying and pulling the vitreous gel away from the retina may be sufficient to release the adhesion. However, in stronger, larger surface area adhesions, this study predicts that enzymatic vitreolysis could exacerbate existing symptoms if the traction does not release after treatment.

Interest also is growing in the use of enzymes to alter the vitreous in an attempt to treat diabetic macular edema and neovascular AMD.[54,55] Degrading and reducing the elasticity of the vitreous body could prove useful in the case of vitreoretinal neovascularization, as in vitro experiments have shown that the number and length of angiogenic sprouts decreases in softer collagen matrices.[56] However, if traction is simultaneously increased in the posterior vitreous, it is possible that an increase in mechanical tension (similar to that imposed by a posterior vitreomacular adhesion) could enhance neovascular AMD progression.[57–59] Similarly, increased vitreomacular traction caused by increased alignment of collagen fibrils could increase the risk of retinal detachment or macular hole formation. Clearly, more clinical and basic research is warranted in this area to determine the safety and efficacy of enzymatic vitreolysis in treating these diseases.

In summary, we demonstrated the utility of using QPLI as a tool to map fiber organization in the vitreous at both a global and local level. Our results suggest that proteoglycan degradation leads to gross remodeling of vitreous fibers, increasing microscopic fiber alignment and reducing angular variability throughout the sample. These results suggest that a more general mechanism of vitreous degeneration may play an important role in the resolution of tractional vitreoretinal adhesions following enzymatic vitreolysis. More studies are warranted to better understand how changes in collagen organization and vitreous architecture correlate with changes in stresses applied at the vitreoretinal interface.

Acknowledgments

We thank Rajendra Apte, MD, PhD (Washington University School of Medicine, Ophthalmology) for helpful discussions. This study was supported by the National Eye Institute (EY013360 [BAF]; Core Grant EY02687), the Howard Hughes Medical Institute (Summer Undergraduate Research and Summer Scholars in Biology and Biomedical Research Fellowships [NSS]), the Washington University Bear Club Fund for Translational Research (DCB), and an unrestricted grant from Research to Prevent Blindness to the Department of Ophthalmology and Visual Science.

Disclosure: **B.A. Filas**, None; **N.S. Shah**, None; **Q. Zhang**, None; **Y.-B. Shui**, None; **S.P. Lake**, None; **D.C. Beebe**, None

References

1. Filas BA, Zhang Q, Okamoto RJ, Shui Y-B, Beebe DC. Enzymatic degradation identifies components responsible for the structural properties of the vitreous body. *Invest Ophthalmol Vis Sci*. 2014;55:55–63.
2. Sebag J. Anomalous posterior vitreous detachment: a unifying concept in vitreo-retinal disease. *Graefes Arch Clin Exp Ophthalmol*. 2004;242:690–698.
3. Bos KJ, Holmes DF, Meadows RS, Kadler KE, McLeod D, Bishop PN. Collagen fibril organisation in mammalian vitreous by freeze etch/rotary shadowing electron microscopy. *Micron*. 2001;32:301–306.
4. Balazs EA. Physiology of the vitreous body. In: Schepens CL, ed. *Importance of the Vitreous Body in Retinal Surgery with Special Emphasis on Re-operations*. St. Louis, MO: Mosby; 1960:29–57.
5. Los LI, van der Worp RJ, van Luyn MJA, Hooymans JMM. Age-related liquefaction of the human vitreous body: LM and TEM evaluation of the role of proteoglycans and collagen. *Invest Ophthalmol Vis Sci*. 2003;44:2828–2833.
6. Góes RM, Nader HB, Porcionatto MA, Haddad A, Laicine EM. Chondroitin sulfate proteoglycans are structural renewable constituents of the rabbit vitreous body. *Curr Eye Res*. 2005; 30:405–413.
7. Bishop PN, Holmes DF, Kadler KE, McLeod D, Bos KJ. Age-related changes on the surface of vitreous collagen fibrils. *Invest Ophthalmol Vis Sci*. 2004;45:1041–1046.
8. Los LI. The rabbit as an animal model for post-natal vitreous matrix differentiation and degeneration. *Eye*. 2008;22:1223–1232.
9. Eisner G. Clinical anatomy of the vitreous. In: Duane TD, Jaeger EA, eds. *Biomedical Foundations of Ophthalmology.* 1st ed. Philadelphia, PA: Lippincott; 1984:1–34.
10. Sebag J, Balazs EA. Human vitreous fibres and vitreoretinal disease. *Trans Ophthalmol Soc U K*. 1985;104:123–128.
11. Sebag J. Age-related changes in human vitreous structure. *Graefes Arch Clin Exp Ophthalmol*. 1987;225:89–93.
12. Walton KA, Meyer CH, Harkrider CJ, Cox TA, Toth CA. Age-related changes in vitreous mobility as measured by video B scan ultrasound. *Exp Eye Res*. 2002;74:173–180.
13. Rossi T, Querzoli G, Pasqualitto G, et al. Ultrasound imaging velocimetry of the human vitreous. *Exp Eye Res*. 2012;99:98–104.
14. Aguayo J, Glaser B, Mildvan A, Cheng HM, Gonzalez RG, Brady T. Study of vitreous liquifaction by NMR spectroscopy and imaging. *Invest Ophthalmol Vis Sci*. 1985;26:692–697.
15. Piccirelli M, Bergamin O, Landau K, Boesiger P, Luechinger R. Vitreous deformation during eye movement. *NMR Biomed*. 2012;25:59–66.
16. Itakura H, Kishi S, Li D, Nitta K, Akiyama H. Vitreous changes in high myopia observed by swept-source optical coherence tomography. *Invest Ophthalmol Vis Sci*. 2014;55:1447–1452.
17. Itakura H, Kishi S, Li D, Akiyama H. Observation of posterior precortical vitreous pocket using swept-source optical coherence tomography. *Invest Ophthalmol Vis Sci*. 2013;54:3102–3107.
18. Tower TT, Tranquillo RT. Alignment maps of tissues: I. Microscopic elliptical polarimetry. *Biophys J*. 2001;81:2954–2963.
19. Tower TT, Tranquillo RT. Alignment maps of tissues: II. Fast harmonic analysis for imaging. *Biophys J*. 2001;81:2964–2971.
20. Chandran PL, Barocas VH. Microstructural mechanics of collagen gels in confined compression: poroelasticity, viscoelasticity, and collapse. *J Biomech Eng*. 2004;126:152–166.
21. Lake SP, Barocas VH. Mechanical and structural contribution of non-fibrillar matrix in uniaxial tension: a collagen-agarose co-gel model. *Ann Biomed Eng*. 2011;39:1891–1903.

22. Tower TT, Neidert MR, Tranquillo RT. Fiber alignment imaging during mechanical testing of soft tissues. *Ann Biomed Eng*. 2002;30:1221–1233.
23. Lake SP, Miller KS, Elliott DM, Soslowsky LJ. Effect of fiber distribution and realignment on the nonlinear and inhomogeneous mechanical properties of human supraspinatus tendon under longitudinal tensile loading. *J Orthop Res*. 2009;27:1596–1602.
24. Quinn KP, Winkelstein BA. Preconditioning is correlated with altered collagen fiber alignment in ligament. *J Biomech Eng*. 2011;133:064506.
25. Kuszak JR, Zoltoski RK, Tiedemann CE. Development of lens sutures. *Int J Dev Biol*. 2004;48:889–902.
26. Kuszak JR, Zoltoski RK, Sivertson C. Fibre cell organization in crystalline lenses. *Exp Eye Res*. 2004;78:673–687.
27. Stalmans P, Benz MS, Gandorfer A, et al. Enzymatic vitreolysis with ocriplasmin for vitreomacular traction and macular holes. *N Engl J Med*. 2012;367:606–615.
28. Gandorfer A, Rohleder M, Sethi C, et al. Posterior vitreous detachment induced by microplasmin. *Invest Ophthalmol Vis Sci*. 2004;45:641–647.
29. Zhi-Liang W, Wo-Dong S, Min L, Xiao-Ping B, Jin J. Pharmacologic vitreolysis with plasmin and hyaluronidase in diabetic rats. *Retina*. 2009;29:269–274.
30. Gandorfer A. Objective of pharmacologic vitreolysis. *Dev Ophthalmol*. 2009;44:1–6.
31. Bishop PN. Vitreous as a substrate for vitreolysis. *Dev Ophthalmol*. 2009;44:7–19.
32. Van Deemter M, Kuijer R, Harm Pas H, Jacoba van der Worp R, Hooymans JMM, Los LI. Trypsin-mediated enzymatic degradation of type II collagen in the human vitreous. *Mol Vis*. 2013;19:1591–1599.
33. Heuser J. Three-dimensional visualization of coated vesicle formation in fibroblasts. *J Cell Biol*. 1980;84:560–583.
34. Berens P. CircStat: a Matlab toolbox for circular statistics. *J Stat Soft*. 2009;31:1–20.
35. Foos RY. Vitreoretinal juncture; topographical variations. *Invest Ophthalmol Vis Sci*. 1972;11:801–808.
36. Matsumoto B, Blanks JC, Ryan SJ. Topographic variations in the rabbit and primate internal limiting membrane. *Invest Ophthalmol Vis Sci*. 1984;25:71–82.
37. Wang J, McLeod D, Henson DB, Bishop PN. Age-dependent changes in the basal retinovitreous adhesion. *Invest Ophthalmol Vis Sci*. 2003;44:1793–1800.
38. Balazs EA. Functional anatomy of the vitreous. In: Duane TD, Jaeger EA, eds. *Biomedical Foundations of Ophthalmology*. 1st ed. Philadelphia, PA: Lippincott; 1984:1–16.
39. Beebe DC, Holekamp NM, Siegfried C, Shui Y-B. Vitreoretinal influences on lens function and cataract. *Philos Transact B Biol Sci*. 2011;366:1293–1300.
40. Bishop PN. Structural macromolecules and supramolecular organisation of the vitreous gel. *Prog Retin Eye Res*. 2000;19:323–344.
41. Teixeira A, Chong LP, Matsuoka N, et al. Vitreoretinal traction created by conventional cutters during vitrectomy. *Ophthalmology*. 2010;117:1387–1392.e2.
42. Schneider EW, Johnson MW. Emerging nonsurgical methods for the treatment of vitreomacular adhesion: a review. *Clin Ophthalmol*. 2011;5:1151–1165.
43. Liu X, Wang L, Wang C, Sun G, Liu S, Fan Y. Mechanism of traumatic retinal detachment in blunt impact: a finite element study. *J Biomech*. 2013;46:1321–1327.
44. Rangarajan N, Kamalakkannan SB, Hasija V, et al. Finite element model of ocular injury in abusive head trauma. *J AAPOS*. 2009;13:364–369.
45. Hans SA, Bawab SY, Woodhouse ML. A finite element infant eye model to investigate retinal forces in shaken baby syndrome. *Graefes Arch Clin Exp Ophthalmol*. 2009;247:561–571.
46. Sebag J, Balazs EA. Morphology and ultrastructure of human vitreous fibers. *Invest Ophthalmol Vis Sci*. 1989;30:1867–1871.
47. Schaller J, Gerber SS. The plasmin-antiplasmin system: structural and functional aspects. *Cell Mol Life Sci*. 2011;68:785–801.
48. Sebag J, Ansari RR, Suh KI. Pharmacologic vitreolysis with microplasmin increases vitreous diffusion coefficients. *Graefes Arch Clin Exp Ophthalmol*. 2007;245:576–580.
49. Quiram PA, Leverenz VR, Baker RM, Dang L, Giblin FJ, Trese MT. Microplasmin-induced posterior vitreous detachment affects vitreous oxygen levels. *Retina*. 2007;27:1090–1096.
50. Giblin FJ, Quiram PA, Leverenz VR, Baker RM, Dang L, Trese MT. Enzyme-induced posterior vitreous detachment in the rat produces increased lens nuclear pO2 levels. *Exp Eye Res*. 2009;88:286–292.
51. Li Q, Yan H, Ding T-B, Han J, Shui Y-B, Beebe DC. Oxidative responses induced by pharmacologic vitreolysis and/or long-term hyperoxia treatment in rat lenses. *Curr Eye Res*. 2013;38:639–648.
52. Filas BA, Shui Y-B, Beebe DC. Computational model for oxygen transport and consumption in human vitreous. *Invest Ophthalmol Vis Sci*. 2013;54:6549–6559.
53. Ponsioen TL, Hooymans JMM, Los LI. Remodelling of the human vitreous and vitreoretinal interface—a dynamic process. *Prog Retin Eye Res*. 2010;29:580–595.
54. Stefanini FR, Maia M, Falabella P, et al. Profile of ocriplasmin and its potential in the treatment of vitreomacular adhesion. *Clin Ophthalmol*. 2014;8:847–856.
55. De Smet MD, Castilla M. Ocriplasmin for diabetic retinopathy. *Expert Opin Biol Ther*. 2013;13:1741–1747.
56. Mason BN, Starchenko A, Williams RM, Bonassar LJ, Reinhart-King CA. Tuning three-dimensional collagen matrix stiffness independently of collagen concentration modulates endothelial cell behavior. *Acta Biomater*. 2013;9:4635–4644.
57. Krebs I, Brannath W, Glittenberg C, Zeiler F, Sebag J, Binder S. Posterior vitreomacular adhesion: a potential risk factor for exudative age-related macular degeneration? *Am J Ophthalmol*. 2007;144:741–746.
58. Robison CD, Krebs I, Binder S, et al. Vitreomacular adhesion in active and end-stage age-related macular degeneration. *Am J Ophthalmol*. 2009;148:79–82.e2.
59. Simpson ARH, Petrarca R, Jackson TL. Vitreomacular adhesion and neovascular age-related macular degeneration. *Surv Ophthalmol*. 2012;57:498–509.

Investigative Ophthalmology & Visual Science